Journal of Structural Geology, Vol. 13, No. 3, pp. 299 to 318, 1991
Printed in Great Britain

0191-8141/91 $03.00+0.00

Intense non-coaxial shear and the development of mega-scale sheath folds in the Arunta Block, Central Australia

B. GOSCOMBE*

Department of Geology, Melbourne University, Parkville, Victoria 3052, Australia

(*Received* 5 *July* 1989; *accepted in revised form* 30 *July* 1990)

Abstract—The Strangways Orogenic Belt of 1800 Ma granulites in the central Arunta Block was completely reworked at granulite-facies grades during the Middle Proterozoic (1400–1500 Ma). The bulk strain regime of the initial episodes of this reworking is presented. Ductile reworking involved non-coaxial deformation on a regional scale and produced map-scale sheath folds. High bulk shear strains are inferred on microscopic and macroscopic scales and the spatial variation in bulk shear strain throughout the region is discussed. The high bulk shear strains were accommodated by east-over-west ductile ramping and fold repetition, resulting in easterly inclined structures, crustal shortening and crustal over-thickening.

INTRODUCTION

GRANULITE gneisses of the Arunta Block (Fig. 1) underwent intense ductile reworking during the Middle Proterozoic (1400–1500 Ma), subsequent to Early Proterozoic metamorphism (1800 Ma). Regional deformation has been named the *Proterozoic reworking* and has been divided into two distinct episodes (Goscombe 1987). Initial reworking involved an episode of inclined progressive shear during compression (D_2–D_3) and was followed by a more upright transpressional episode (D_4–D_5) (Table 1). Initial reworking produced a complex outcrop pattern of steeply inclined sheath folds and refolded sheaths on the map scale. Similar scale sheath folds have been previously described from only a few localities (Henderson 1981, Lacassin & Mattauer 1988, Park 1988, N. Culshaw 1988 personal communication).

This paper presents the first detailed structural analysis undertaken in the Strangways Range. Prior to this, the true nature of the high-grade Proterozoic orogenesis of this portion of the Arunta Block was unknown. This study is based on detailed mapping in the NE Strangways Range and reconnaissance work in granulites from all portions of the Central Tectonic Province (CTP) (Fig. 1). This paper defines the nature of the deformational regime during only the initial stages of the Proterozoic reworking (D_2–D_3) (Table 1). Analysis of the type and sense of shear, and bulk shear strains experienced, is presented and the tectonic framework of deformation discussed.

REGIONAL GEOLOGY AND TECTONIC FRAMEWORK

The NE Strangways Range is a small portion of the E–W-trending belt of CTP granulites named the Strangways Orogenic Belt (James & Ding 1987) (Fig. 1), which is a layered sequence of supra-crustal gneisses. The lithological layering on m- to km-scale is denoted S_0 (Table 1). The sequence is dominated by two pyroxene mafic gneiss and garnet–orthopyroxene–biotite-bearing quartzo-feldspathic gneisses. These have tholeiitic and rhyolitic compositions, respectively, and have field relationships consistent with a bimodal volcanic pile (Warren 1983, Windrim 1983, Stewart *et al.* 1984) which has been dated by Sm–Nd systematics at approximately 2000–2100 Ma (Windrim & McCulloch 1986). Interlayered with the volcanic pile are indisputable meta-supracrustals such as banded iron formation, quartzite, carbonates, calc-silicates and a wide variety of aluminous and meta-pelitic gneisses (Fig. 2).

Prior to the development of the first recognized tectonic fabrics (S_2–L_2), the Strangways Range supracrustals were buried to 21–25 km depth and subjected to peak temperatures of 850–950°C (Warren 1983, Goscombe 1989) at 1800 Ma (Black *et al.* 1983, Windrim & McCulloch 1986). This granulite-facies metamorphism (M_1) was responsible for the total recrystallization of the whole region to medium- to coarse-grained (0.1–60 cm) polygonal granoblastic and porphyroblastic textures. Fine-scale (mm to tens of cm) compositional gneissic layering and quartzo-feldspathic partial melt segregations were developed during M_1, both constitute S_1 and are concordant with lithological layering (S_0). Units of quartzo-feldspathic gneiss were variably migmatized during M_1, some were completely melted giving rise to large concordant *in situ* granitic orthogneiss units (Goscombe 1989).

As a consequence of M_1 annealing, deformational structures and kinematic indicators from the tectonic episodes responsible for burial to, and metamorphism in, the middle-lower crust, have not been recognized.

M_1 mineral parageneses record an anticlockwise P–T path from lower pressure conditions (Goscombe 1989). Retrogressive reaction coronas and symplectites record an isobaric cooling path to at least 700°C with concomitant partial hydration (Warren 1983, Goscombe 1989).

*Present address: Tasmanian Department of Mines, P.O. Box 56, Rosny Park, Tasmania 7018, Australia.

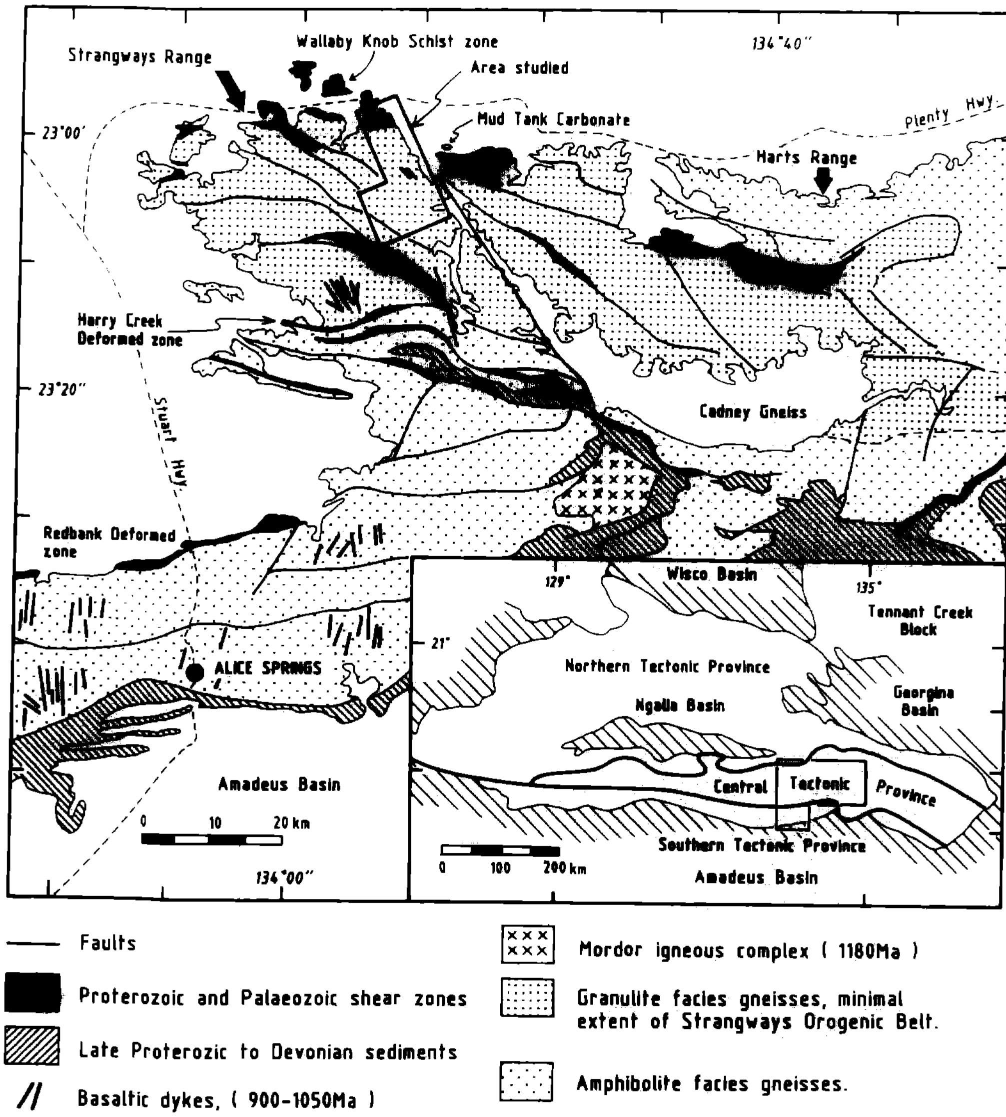

Fig. 1. Regional geological features (based on Shaw & Wells 1983) and locality of area studied. Inset of the tectonic provinces of the Arunta Block and adjacent Proterozoic–Palaeozoic sedimentary basins.

Pervasive post-M_1 hydration was responsible for the crystallization of significant amounts of biotite, phlogopite, hornblende and gedrite at approximately 1670–1720 Ma (Allen & Stubbs 1982, Windrim & McCulloch 1986). Retrogressive fluids were sourced from crystallizing *in situ* partial melts (Hensen & Warren 1985) and produced the metasomatic signatures that are characteristic of the Arunta Block granulites (Allen 1979, Goscombe 1984, 1989).

Both granulite gneisses and granitic orthogneisses were completely reworked, subsequent to M_1, by intense ductile deformation (D_2–D_5) on a regional scale at approximately 1400–1500 Ma (Goscombe 1989). To avoid confusion with previous Arunta Block literature, orogenesis of the Strangways Orogenic Belt has been termed the *Proterozoic reworking*, which comprises two distinct periods of contrasting style of deformation (Table 1). These are:

(1) D_2–D_3: progressive non-coaxial shear with the development of two definable isoclinal fold generations and intense layer-parallel L_2–S_2 tectonic fabric. The nature of D_2–D_3 deformation is the subject of this paper;

(2) D_4–D_5: upright folds (F_4), syn-tectonic granite emplacement at 1430–1490 Ma (Fig. 2 and Table 1) and steeply inclined granulite-facies shear zones (S_5), all formed essentially coevally as a result of regional scale, E–W-trending, sinistral transpression.

All episodes of the Proterozoic reworking occurred under granulite-facies conditions (M_2 and M_5, Table 1). M_2 occurred at higher pressures (>9 kbar) and lower temperatures (800–850°C) than M_1. Mineral parageneses in S_5 shear zones (M_5) record a retrogressive decompression P–T path from 850°C and 9 kbar to 600°C and 6.5 kbar (Goscombe 1989). Thus M_2 and M_5 outline a clockwise P–T path during the Proterozoic reworking, involving burial during D_2–D_3 and decompression to middle crustal levels during the later transpressional (D_4–D_5) phase.

The Strangways Orogenic Belt remained at depth throughout the Late Proterozoic and Early Palaeozoic,

Table 1. Simplified framework of tectonic events experienced in the NE Strangways Range

Igneous events	Metamorphism	Deformation and fabrics		Age (Ma) [Ref.]*
Supracrustal rocks and volcanic deposits		S_0—lithological layering		2100–2000 [1]
Migmatites and *in situ* granitic orthogneiss	M_1—granulite facies, anticlockwise P–T path	S_1—gneissic layering	Lithospheric extension?	1800–1750 [1,2]
	Proterozoic reworking			
	M_2—granulite facies ↓ clockwise P–T path	D_2—isoclines and sheaths D_3—isoclines and sheaths	Non-coaxial ductile crustal shortening	1500–1400 [3,4,5]
	M_5—lower granulite	D_4—open folds D_5—shear zones	Transpression	1490–1425 [2,6]
	Late Proterozoic events			
Dolerite dykes	M_6—Amphibolite facies isobaric heating and cooling			1050–900 [3,7]
Pegmatites and granites		D_6—shear zones	Lithospheric extension	1050–930 [2,8,9]
	Alice Springs Orogeny			
	M_7—amphibolite to greenschist facies, clockwise P–T path	Wallaby Knob Schist Zone	Intra-continental crustal shortening and uplift	>400 [10]
Pegmatites				340–310 [11]

*[1] Windrim & McCulloch 1986; [2] Black *et al.* 1983; [3] Allen & Stubbs 1982; [4] Iyer *et al.* 1976; [5] Woodford *et al.* 1975; [6] Black 1980; [7] Black *et et al.* 1980; [8] Allen & Black 1979; [9] Marjoribanks & Black 1974; [10] Collation of published cooling ages (Goscombe 1989); [11] Mortimer *et al.* 1985.

experiencing limited crustal extension and the emplacement of scattered dolerite dykes. The granulites were exposed prior to the Tertiary (Wells & Moss 1983) as a consequence of the intra-continental (Teyssier 1985) Alice Springs orogeny (Forman 1971, Shaw *et al.* 1984a) at approximately 400 Ma (Table 1).

D_2–D_3 STRUCTURAL ELEMENTS

Two episodes of isoclinal folding, on all scales (mm- to km-scale), are recognized in the NE Strangways Range. F_2 folds, the earliest deformational structures, are defined as those with a penetrative axial planar L_2–S_2 fabric (Fig. 3a). Whereas F_3 folds refold both F_2 folds and the regional L_2–S_2 fabric without penetrative fabric development (Figs. 4a & b).

Mesoscopic fold structures

F_2 folds are tight to isoclinal, have rounded and thickened hinges and attenuated limbs (Fig. 3a), with fold axes parallel to the mineral elongation lineation (L_2). Mesoscopic F_2 folds are both intrafolial within and fold the lithological layering (S_0). Asymmetrical mesoscopic folds (Fig. 3b) define a sense of vergence (Bell 1981) which is consistent with the macroscopic F_2 closures (Fig. 7), thus implying the coeval generation of both these scales of folding.

Mesoscopic F_2 sheath folds are common in macroscopic F_2 hinge regions and best developed in quartzofeldspathic gneiss (Fig. 3c). Cross-sections normal to the sheath fold long axes have flattened ellipse shapes with orthogonal dimensions of 1–8 cm by 2–20 cm with shape ratios (B/C, Fig. 8) ranging from 2 to 6. The long axes of sheath folds are parallel to the mineral elongation lineation (L_2) (Fig. 3d) and up to 50 cm long. Throughout their length there is only minimal change in the cross-sectional area of sections orthogonal to the sheath long axis (Fig. 8). The plane of sheath flattening is parallel to the tectonic fabric (S_2). There appears to be a predominance of antiformal sheaths as a result of their having more rounded noses, whereas synforms are typically sheared out. Sheath terminology and the relationship between D_2 tectonic fabrics and F_2 fold geometry are summarized in Fig. 9.

F_3 folds are isoclinal with rounded hinges. Hinge thickening and limb attenuation is not as pronounced as in the F_2 folds. A crenulation lineation, defined by mm-scale parasitic folds, is developed parallel to F_3 fold axes. Mesoscopic F_3 sheath folds have irregular cross-section shapes (Fig. 4c) and are commonly developed in the tightest macroscopic F_3 hinge regions.

F_2 and F_3 folds are nearly co-planar and co-linear (Fig. 10), both plunge steeply (50–80°) towards the NE and SE and are inclined 50–80° to the ESE. F_2 fold axes and the long axes of sheaths are contained within the plane of the regional tectonic foliation (S_2) and tightly scattered symmetrically around the average L_2 orientation. F_3 fold axes are more widely scattered around the average L_2 direction than F_2 folds (Fig. 10).

Macroscopic fold structures

Macroscopic F_2 structures are very tight to isoclinal with rounded hinges (Fig. 11). Large-scale lithological

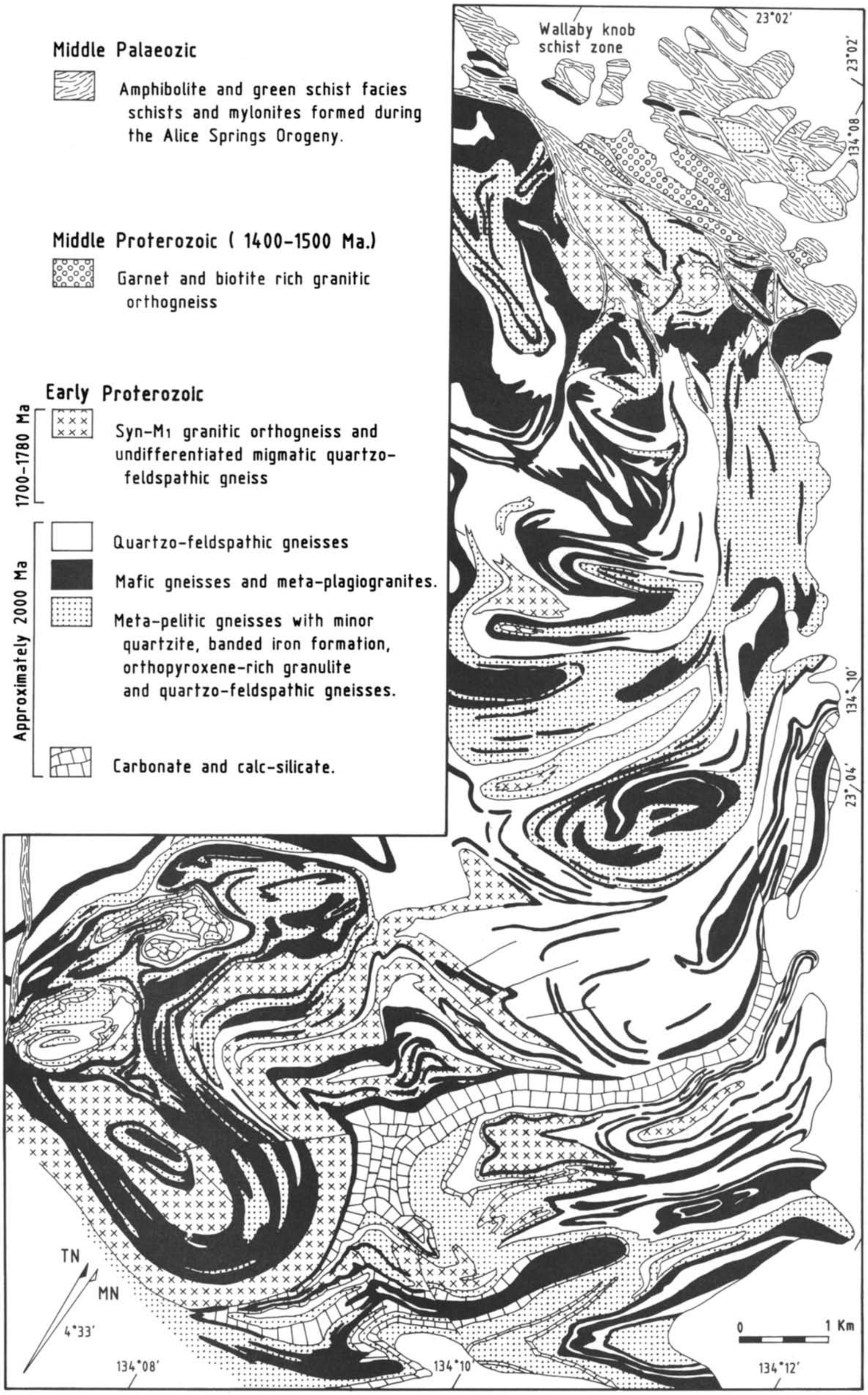

Fig. 2. Simplified lithological map of the NE Strangways Range.

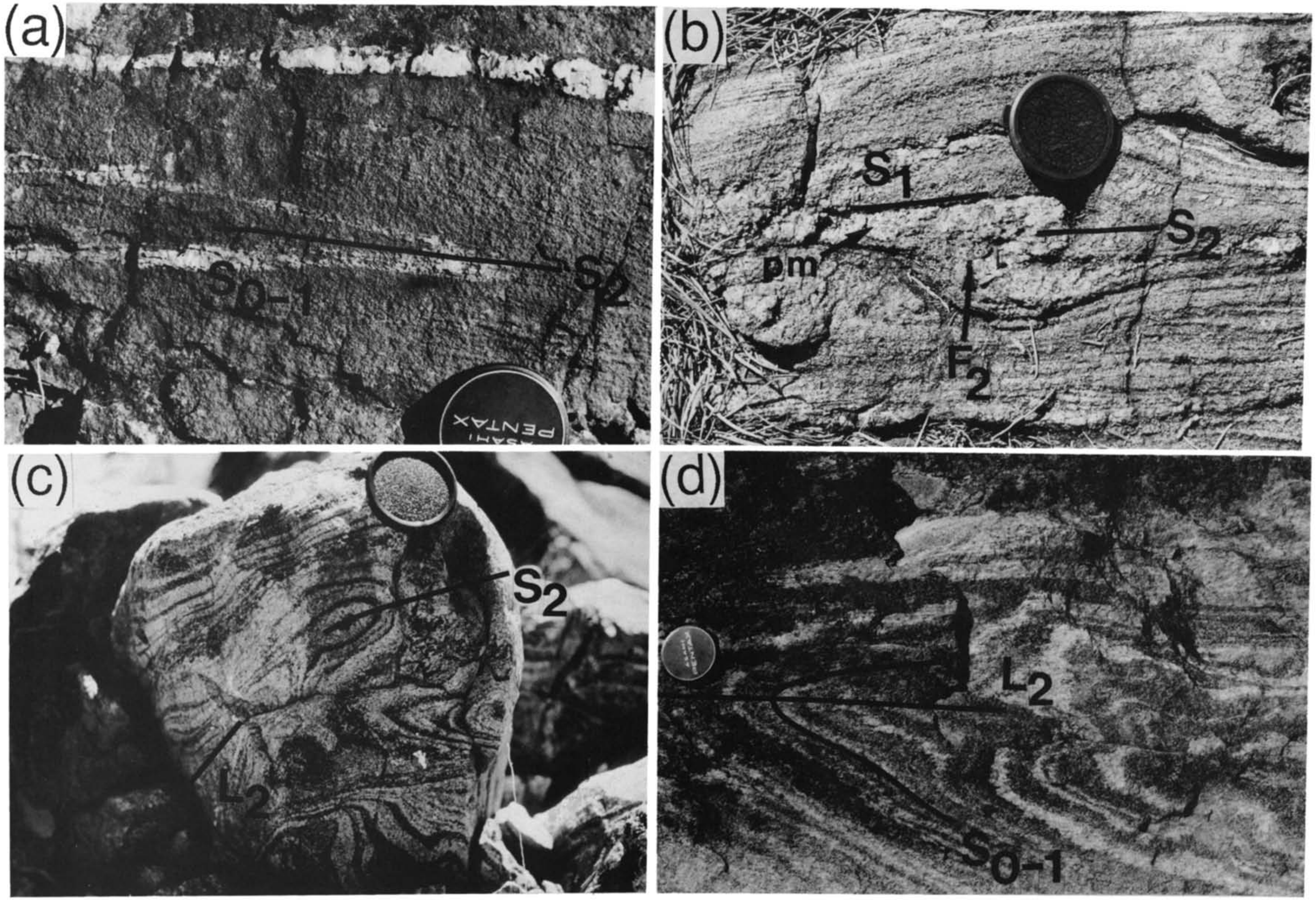

Fig. 3. (a) Intra-folial F_2 isoclinally folded quartz layer in mafic gneiss, note axial planar tectonic fabric (S_2) of quartz-aggregate ribbon. (b) Asymmetrically folded (F_2) M_1 partial melt segregation displaying dextral vergence and fold axial planar fabric (S_2) development. (c) F_2 sheath fold in quartzo-feldspathic gneiss. Note flattened ellipse shaped cross-section and relationship to S_2–L_2 structural elements. (d) XY section through sheath fold (in plane of S_2) illustrating extreme stretching of gneissic layering into near parallelism with L_2. Lens cap is 50 mm.

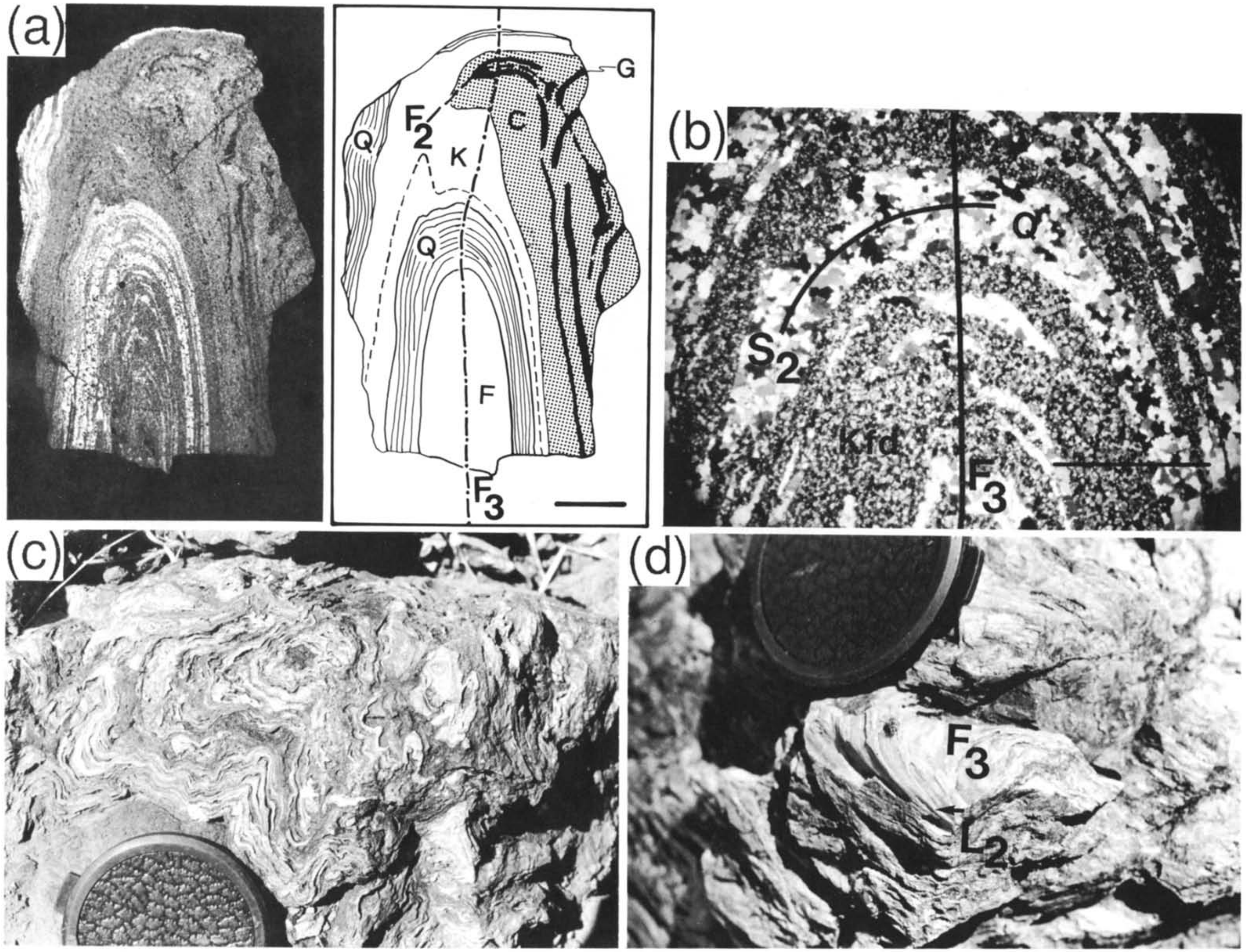

Fig. 4. (a) Micro-photograph and sketch of isoclinal F_3 closure in ultra-mylonitic (S_2) calcareous meta-pelite. Note F_3-refolding of F_2 closure in garnet-rich layer (G). (F) feldspar-aggregate ribbons, (Q) quartz-aggregate ribbons, (K) garnet–hornblende–biotite–orthopyroxene–quartz–plagioclase, (C) assemblage as in (K) without hornblende. Bar scale is 3 cm. (b) Micro-photograph of F_3 closure in (a). Note quartz and feldspar grains, in aggregate ribbons, show no internal deformation. Bar scale is 1 cm. (c) Spectacular F_3 sheath folds in S_2 ultra-mylonitic calcareous meta-pelite. (d) Marginal hinge of F_3 sheath refolding quartz-aggregate stretching lineation (L_2).

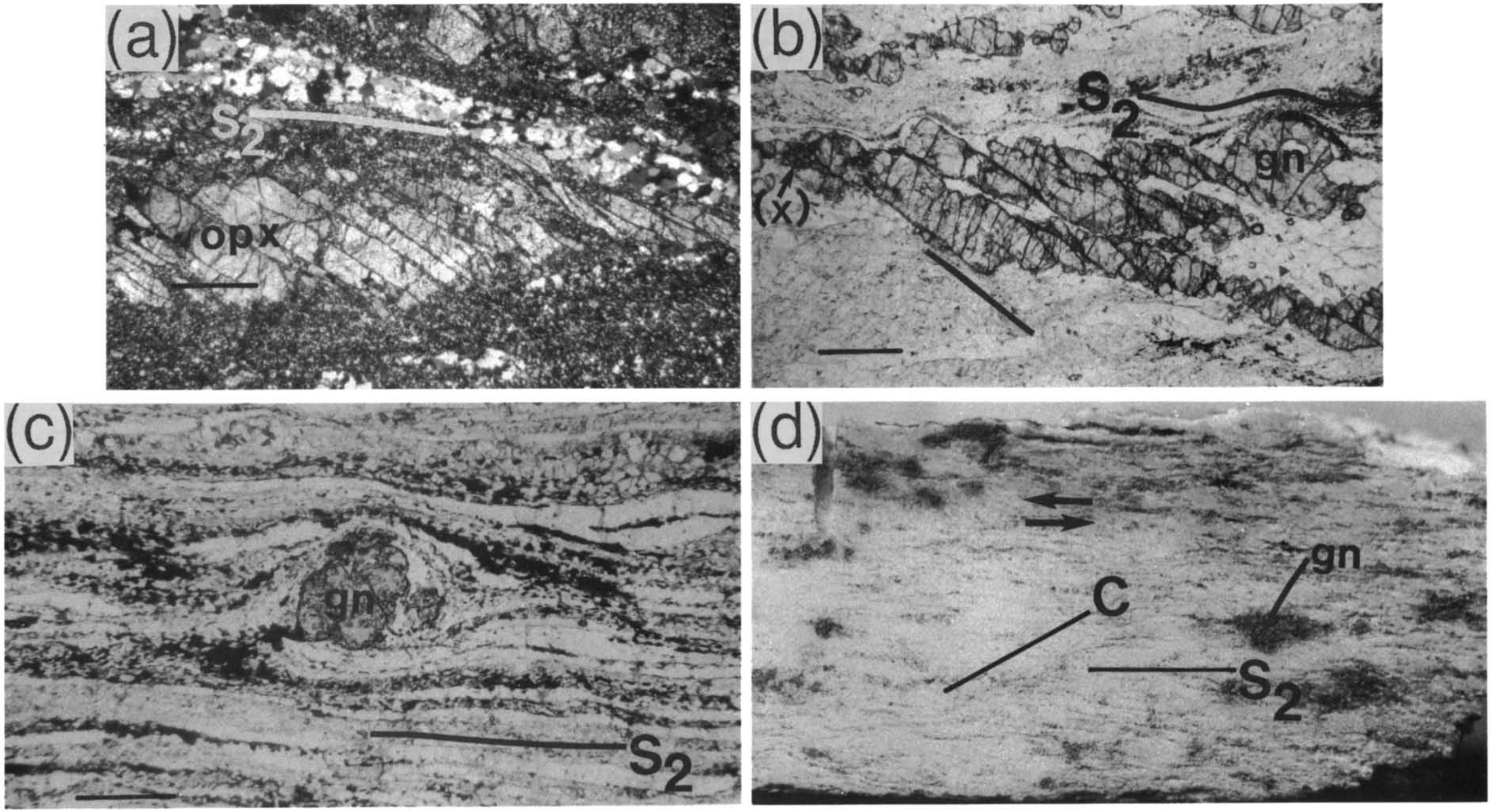

Fig. 5. (a) Grain refinement at the margin of asymmetrically stretched M_1 orthopyroxene in meta-ironstone. Stretching is accommodated by normal movements along micro-faults of fine-scale recrystallization. Displacements along micro-faults define a sinistral sense of shear. (b) Fine-grained recrystallization of M_1 garnet in pressure shadow (x). Extreme asymmetrical stretching of porphyroblast, by slip along micro-faults, defines a sinistral sense of shear. (c) S_2 asymmetrically enclosing σ-type M_1 garnet porphyroblast, with minor rotation of garnet and pressure shadow defining dextral sense of shear. Intense S_2 mylonitic fabric is defined by planar quartz-, feldspar- and opaque-ribbons and biotite platelets. (d) *S–C* mylonite in quartzo-feldspathic gneiss, defining sinistral sense of shear. Large acute angle between S_2- and *C*-planes imply low shear strain. *All bar scales are 1 mm.* All sections are cut parallel to L_2 and orthogonal to S_2 and photographed in plane polarized light.

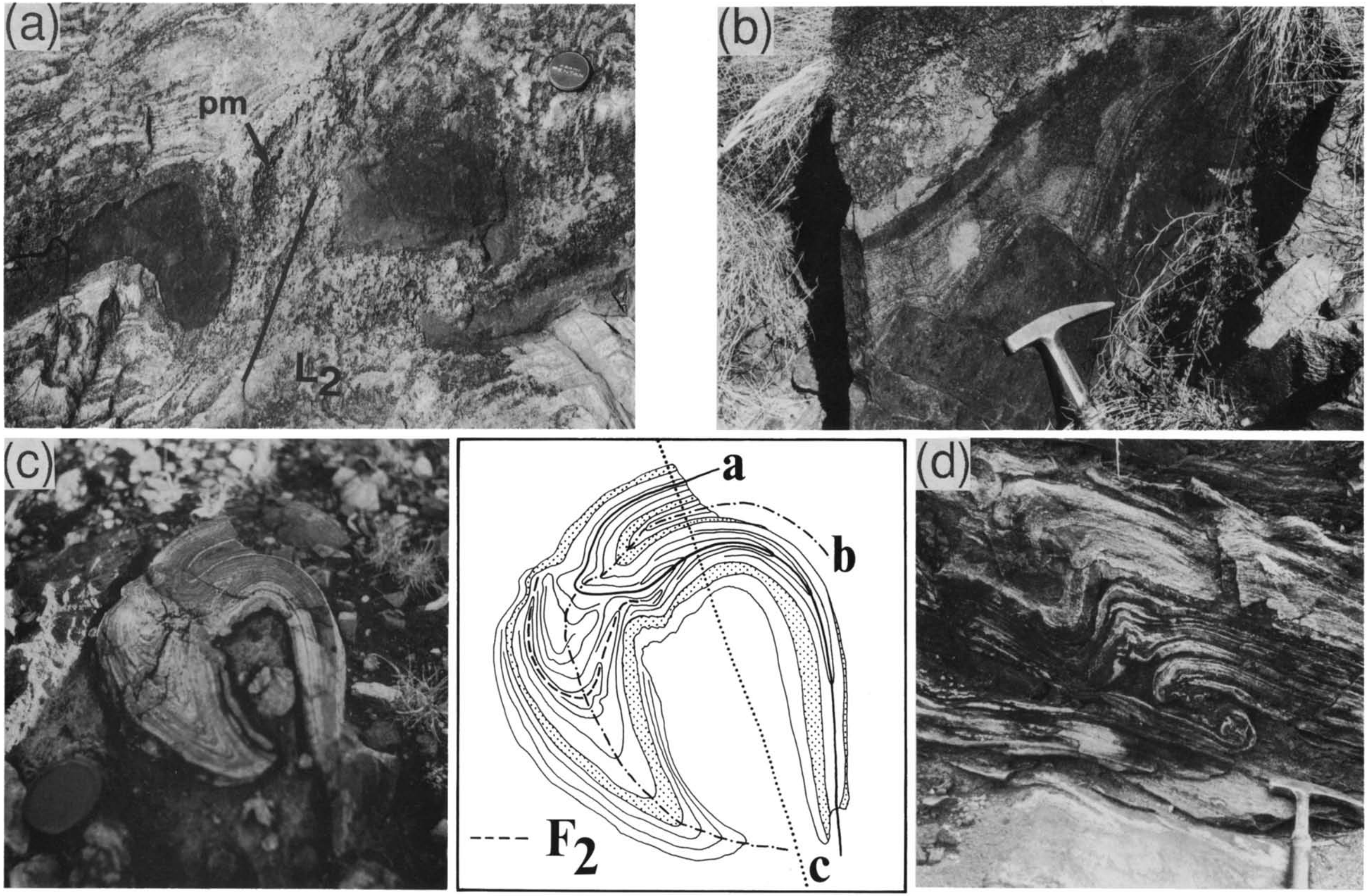

Fig. 6. (a) D_2 boudinage, of mafic gneiss, parallel to intense L_2 fabric. Note quartzo-feldspathic segregation infilling between boudins and extension orthogonal to L_2. (b) Asymmetrical extension of mafic gneiss accommodated by normal offsets and block rotation defining sinistral shear. Note very ductile nature of deformation in enclosing quartzo-feldspathic gneiss. (c) Sketch and photograph of three phases of F_3 folding of S_2 calc-silicate ultra-mylonite (F_3 folds labelled successively a, b and c). Note last phase of folding has folded earlier closures through approximately 252° and note the extreme ductile thinning of S_2, resulting in an isolated 'rolling' structure within a carbonate matrix. (d) Development of a ball shaped 'rolling' structure by sinistral, east-over-west, shear in inter-layered calc-silicate and marble rock. Location in the Cadney gneisses (Fig. 1) (Goscombe 1984).

layering (S_0) is folded around F_2 closures, whereas intense S_2 fabric development, in quartzo-feldspathic and pelitic lithologies, masks pre-existing mesoscopic gneissic layering (S_1) in the hinge regions. This destruction of gneissic layering, makes the recognition of map-scale F_2 hinge regions difficult.

Macroscopic F_2 structures have two distinct outcrop geometries;

(1) plunging, inclined isoclinal folds (Fig. 11) with axial surfaces parallel to the regional S_2 foliation and with fold axes sub-parallel to the regional L_2 orientation (Figs. 10 and 11);

(2) F_2 structures form km-scale closed outcrop patterns with flattened ellipse shaped horizontal sections (Figs. 2 and 11). Marginal hinges (Fig. 9) at both ends of these closed structures plunge sub-parallel to each other and are parallel to the fold axes of adjacent macroscopic F_2 folds and L_2 (Figs. 10 and 11). The marginal hinges of these structures meet either above or below the surface of outcrop (at the terminal closure or 'nose') to be consistent with the closed outcrop patterns (Figs. 2 and 11). As such, these structures define an elongate and flattened sheath fold geometry. The inter-marginal hinge angle (Fig. 8) of these mega-sheaths range 6–34° and the degree of ellipticity (B/C), of sections orthogonal to their length, range from 2.2 to 8.5. Like mesoscopic sheath folds, these structures are flattened in the regional S_2 foliation and elongate parallel to L_2.

Macroscopic F_3 sheaths have flattened elliptical cross-sections similar to F_2 sheath folds (Fig. 11). L_2 lineations are refolded by mesoscopic (Fig. 4d) and macroscopic F_3 folds, resulting in nearly co-linear L_2 orientations on both F_3 limbs (C, Fig. 11). Schematic representation of the F_3 refolding of D_2 structural elements is summarized in Fig. 9. Of significance is the common occurrence of large bodies of M_1 orthogneiss and mafic gneiss in the cores of sheath folds (Fig. 2), suggesting that these inhomogeneities in the gneissic pile controlled nucleation of the fold (Minnigh 1979, Berthé & Brun 1980, Cobbold & Quinquis 1980).

The three-dimensional geometry of individual F_2 and F_3 sheath folds cannot be the result of fold interference between any number of cylindrical folds formed in a coaxial deformational environment. This is illustrated by the development of isolated sheath structures. For example, the axis of symmetry, orthogonal to the fold axial plane (S_2), does not extend beyond the margin of individual sheath fold into adjacent ones with the same sense of closure along its length (domain G, Fig. 12). Thus this axis cannot be a second-stage fold axis of a dome and basin pattern of two isoclinal fold events. Furthermore, the sub-parallel nature of marginal hinges and sides of sheath folds, as well as the same shear sense on each limb, are incompatible with their generation by refolding of two or more coaxial fold generations. Consequently, these structures are true sheaths and must have involved stretching and rotation of the marginal fold hinge into parallelism with L_2. Other examples of sheaths developed on a similar scale exist, for example; Hudsonian Orogen in northeast Canada (Henderson 1981), the Swiss Alps (Lacassin & Mattauer 1985), Svecokarelides, eastern Finland (Park 1988) and potential structures in the Grenville Province, Canada (N. Culshaw 1988 personal communication).

Refolding of macroscopic F_2 fold structures by F_3 folds, gave rise to complex fold interference patterns (Figs. 2 and 11). Three-dimensional interpretation of two regions of macroscopic F_2 and F_3 fold interference, from domains D and F (Fig. 10), are presented (Fig. 12). These F_2–F_3 interference patterns have no analog with the classical interference patterns of Ramsay (1967) and Thiessen (1986), because of the non-coaxial nature of deformations involved (see later discussion) and the co-linearity of both F_2 and F_3 structures. The F_2–F_3 interference pattern is more analogous (though on a larger scale) to that observed in ductile shear zones that have undergone progressive non-coaxial shear (Berthé & Brun 1980, Cobbold & Quinquis 1980).

D_2 *tectonic fabrics and microstructure*

A very pronounced L_2–S_2 tectonic fabric is developed throughout the region. The regional elongation lineation (L_2) is defined in pelitic, quartzo-feldspathic and calc-silicate gneisses by elongate lenses of quartz-aggregate (Fig. 6a), boudinaged and stretched feldspar, orthopyroxene and garnet porphyroblasts (Figs. 5a & b), elongate pressure shadows consisting of aggregates of quartz, feldspar and biotite, and by fine-grained prismatic sillimanite. In mafic gneiss, L_2 is defined by elongate pressure shadows consisting of fine-grained aggregates of hornblende, plagioclase and pyroxene.

L_2 is sub-parallel to F_2 sheath folds on all scales (Figs. 3d and 7). Despite two subsequent fold generations, L_2 orientation is tightly constrained throughout the region; plunging 60° towards 100° (Fig. 10). Thus L_2 accurately outlines the direction of transport during D_2.

The pervasive tectonic foliation (S_2), is defined by intense grain size reduction of pre-existing textures. S_2 typically parallels the gneissic and lithological layering (S_0–S_1) (Fig. 10), but overprints S_0–S_1 in F_2 fold hinges (Figs. 3a & d). S_2 is coeval with F_2 folding because of its axial planar development (Figs. 3a and 8). S_2 is defined by the preferred shape orientation of biotite, gedrite and sillimanite, elongate pressure shadow tails and by planar to lenticular ribbons of fine-grained aggregates of quartz, feldspar, garnet and pyroxene (Figs. 4b and 5a–c). These aggregate ribbons formed by recrystallization, at grain boundaries, of M_1 phases. No undulose extinction or any other deformational feature is preserved in L_2–S_2 aggregate mineral grains (Fig. 4b).

In meta-pelites, quartzo-feldspathic gneisses and orthopyroxene-rich granulite, the L_2–S_2 fabric is mylonitic to proto-mylonitic with up to 100% grain refinement. Quartz and feldspar ribbons (Figs. 4a and 5c) in these lithologies are laterally extensive (on cm-scale) and thin (0.05–1.3 mm). Grain refinement in meta-pelitic gneisses and orthopyroxene-rich granulite is typically 60–95%, resulting in S_2 being the only recognizable planar fabric, other than partial melt segregations. Such

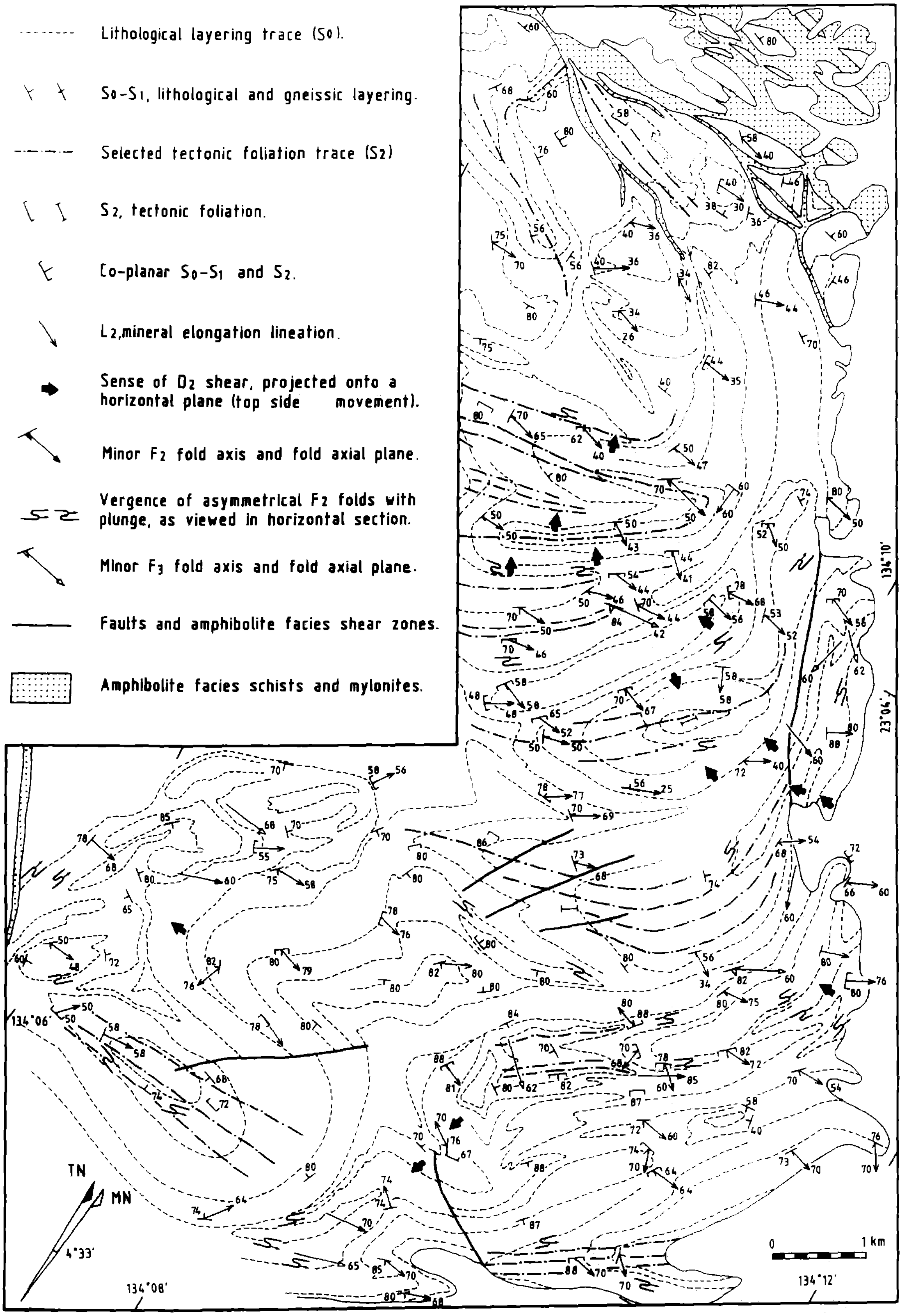

Fig. 7. Simplified structural data map of the NE Strangways Range, for D_2–D_3 structural elements only.

intense grain refinement gives rise to a texture of isolated M_1 porphyroblasts within a fine-grained foliated and lineated matrix (Figs. 5c & d).

Mafic and calc-silicate gneisses display little or no grain refinement. Where present, grain boundary recrystallization defines an incipient S_2 fabric. In the hinges of folded mafic gneisses, S_2 fabrics are more intense, though grain refinement is not as great as experienced by

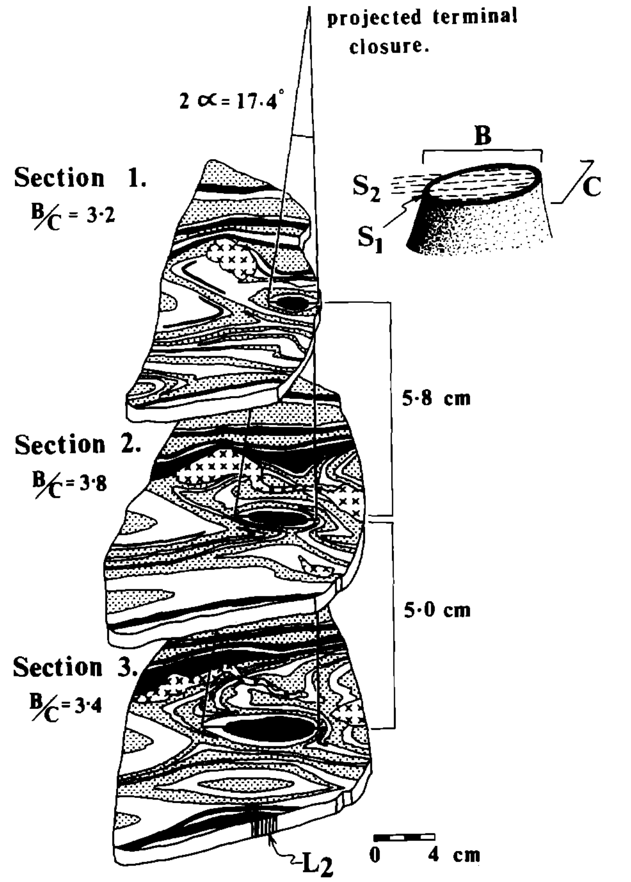

Fig. 8. Tracings of gneissic layering (S_1) in spaced sections through a sheath fold in quartzo-feldspathic gneiss. Sections are normal to L_2. Note late-D_2 partial melt segregations elongate parallel to L_2. Bulk shear strain calculations based on the intermarginal hinge angle (2α) and degree of ellipticity (B/C) of this sheath are defined by the relationship; $\alpha = \arctan[(B/C)\cdot(\gamma^2+1)^{-1}]$ (Lacassin & Mattauer 1985). Shear strain estimates are; section (1) $\gamma = 21$, section (2) $\gamma = 25$, section (3) $\gamma = 22$, averaging $\gamma = 23$.

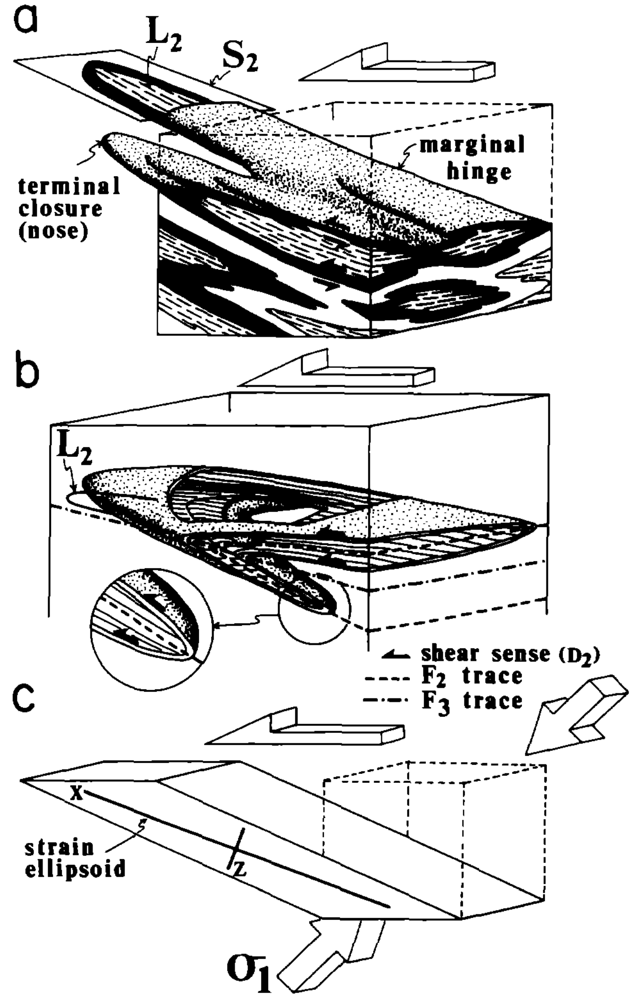

Fig. 9. Schematic block diagrams summarizing: (a) D_2 structural elements, (b) F_3 folding of D_2 structural elements, (c) the idealized relationship between a general (σ_1) finite strain ellipsoid for D_2–D_3 and principal compressive stress in a simple shear environment.

typical mylonites (i.e. <50%). In domain C (Fig. 10), however, the S_2 fabric in mafic gneisses is mylonitic (>50% grain refinement) and asymmetrically encloses M_1 mineral grains.

C-planes (Berthé *et al.* 1979) are developed at low angles (7–25°) to the S_2 foliation (Fig. 5d) in the least deformed quartzo-feldspathic and meta-pelitic gneisses. However, *C*-planes are commonly absent in intensely mylonitized quartzo-feldspathic and meta-pelitic gneisses and orthopyroxene-rich granulite. In these cases, the laterally continuous nature of quartz and feldspar ribbons (>>4 cm) comprising S_2 may be parallel to the plane of shear (*C*-planes).

In thin-section, M_1 orthopyroxene, K-feldspar and plagioclase porphyroblasts are asymmetrically stretched into highly elongate augen. Stretching is accommodated by normal displacements along high-angle micro-faults (Etchecopar 1974, 1977, Platt & Vissers 1980, Simpson 1984), defined by thin (<0.05 mm) planar zones of sub-grains (Fig. 5a). Garnets are also stretched, but develop sharper micro-faults with less sub-grain crystallization (Fig. 5b).

In addition to grain boundary recrystallization of pre-existing phases, new minerals are developed within the S_2 fabric, e.g. gedrite, anthophyllite, biotite, orthopyroxene and sillimanite in orthopyroxene-rich granulite and meta-pelitic gneisses, and garnet, scapolite, hornblende and biotite in quartzo-feldspathic and mafic gneisses. The development of new phases within S_2 fabrics is indicative of M_2 assemblages having crystallized, not only in response to deformation, but under different metamorphic conditions to M_1 (Goscombe 1989).

D_3 *microstructure*

No new mineral phases crystallized during D_3, nor was there any grain refinement. Biotite platelets, quartz-aggregate and feldspar-aggregate ribbons, aligned in S_2, are isoclinally folded by F_3 folds. However, no undulose extinction or kinking of S_2 mineral grains is apparent (Fig. 4), nor alignment of S_2 mineral grains within the F_3 axial plane. Thus the deformational features inherited by S_2 mineral grains during D_3 must have been annealed out subsequent to F_3 folding.

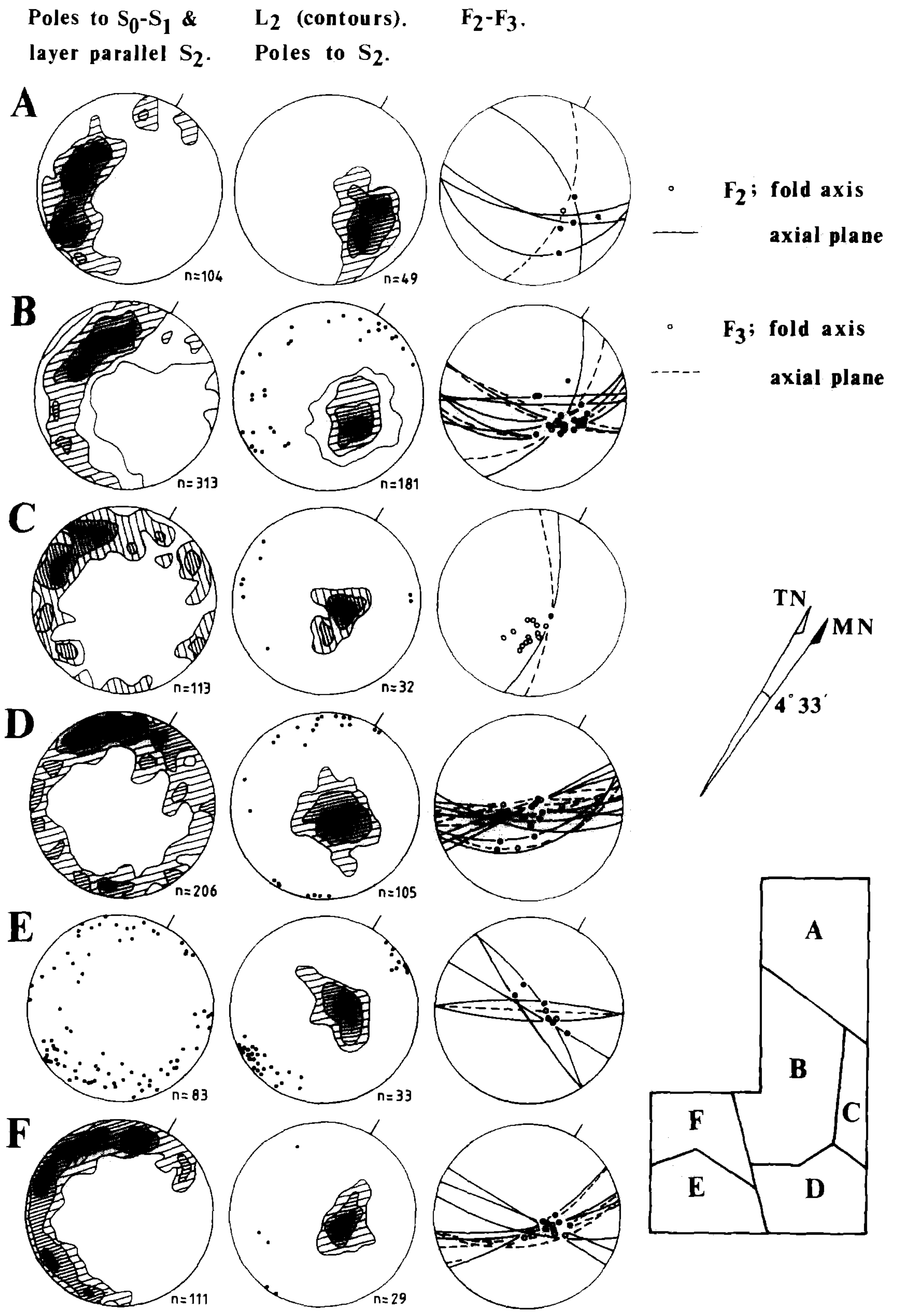

Fig. 10. Lower hemisphere, equal-area, stereographic projections of structural data from the domains outlined in the inset.

D_2 boudinage

Boudinage, within the plane of S_2, occurs on all scales (mm to hundreds of m). Outcrop boudins and boudinaged mineral grains (Figs. 5a & b and 6a) indicate L_2 as the axis of maximum elongation. This is further supported by the highly elongate shape ($X/Z \gg 4$) of mafic xenoliths in quartzo-feldspathic orthogneiss, where their long axes parallel L_2. Only minor boudin separation orthogonal to L_2 within the S_2 plane is noted on a mesoscopic (Fig. 6a) scale but absent on a microscopic (mineral grain) scale, thus deformation is considered close to plane strain.

D_2–D_3 *partial melts*

Small volumes of post-M_1 anhydrous quartz–feldspar segregation occur in a variety of textural relationships. These include; thin (3–12 mm) planar segregations that are sub-parallel to the axial surface of mesoscopic F_2 folds, elongate shaped bodies aligned parallel with the long axis of mesoscopic sheaths in highly sheared quartzo-feldspathic gneisses (Fig. 8) and infillings between boudins (Fig. 6a). As such, the melts collected in zones of maximum dilation associated with D_2 structures. Such alignment of post-M_1 segregations with D_2 structural elements, suggests that minor anhydrous melting occurred during D_2. Some of these segregations develop S_2–L_2 fabrics (Fig. 6a), while others do not (Fig. 8). Thus partial melting and melt crystallization continued subsequent to D_2.

Coarse-grained (1–20 mm), orthopyroxene-bearing charnockite segregations in quartzo-feldspathic gneisses, cross-cut F_3 structures and do not develop S_2 fabrics. These segregations are interpreted to be late-D_3 partial melts. Their presence, along with post-D_2 partial melts, suggests that D_2–D_3 deformation was on a prograde (M_2) metamorphic path and that the peak of metamorphism during the Proterozoic reworking (M_2) was attained subsequent to D_2–D_3.

NATURE OF D_2–D_3 DEFORMATION

Coaxial vs non-coaxial shear

There are two general end-member cases of homogeneous deformation, not involving spin (Lister & Williams 1983); rotational or non-coaxial shear (simple shear) and irrotational or coaxial shear (pure shear) (Hobbs *et al.* 1976). Natural deformational systems experience a combination of these two end-members, though one may predominate over the other (Bell 1978, Lister & Snoke 1984). The significance of non-coaxial deformation during the development of discrete shear zones is universally accepted (Bell 1978, Simpson 1984, Choukroune *et al.* 1987). Whereas, on a regional scale, the bulk strain regime (Choukroune *et al.* 1987) of portions of orogens is rarely quantified (Sandiford 1984, Clarke 1987).

D_2 and D_3 structures, on all scales, preserve evidence for non-coaxial shear. These are as follows.

(1) Boudinage on both mesoscopic and microscopic scale is governed by slip along high-angle micro-faults with normal displacements (Figs. 5a & b and 6b). The same movement sense along consistently inclined micro-faults, must involve rotation of the individual boudins that the faults separate (Etchecopar 1974, 1977). Asymmetrical stretching such as this, is indicative of rotational shear (Simpson & Schmid 1983, Lister & Snoke 1984).

(2) S_2 asymmetrically augens M_1 porphyroblasts (Fig. 5c), with both σ-types, where the foliation asymmetrically encloses a static porphyroblast, and δ-types (or rolling structures, Van Der Driesche & Brun 1987), where the porphyroblast has rotated with respect to the median foliation orientation (Passchier & Simpson 1986). Both asymmetrical geometries are indicative of non-coaxial shear (Choukroune & Lagarde 1977, Berthé *et al.* 1979, Burg *et al.* 1981, Simpson & Schmid 1983, Lister & Snoke 1984, Passchier & Simpson 1986).

(3) *S–C* fabrics are present in the least deformed tectonites, such fabrics are indicative of non-coaxial shear (Berthé *et al.* 1979). The majority of intensely foliated gneisses are interpreted to have co-planar *S–C* fabrics that have formed by high bulk shear strains in a non-coaxial deformational environment (Simpson 1984).

(4) Mesoscopic folds are asymmetrical (Fig. 3b) and intrafolial (Fig. 3a), thus implying rotational shear (Berthé *et al.* 1979, Hanmer 1984).

Sheath folds are commonly reported from shear zones that have experienced non-coaxial shear (Quinquis *et al.* 1978, Minnigh 1979, Berthé & Brun 1980, Cobbold & Quinquis 1980, Henderson 1981, Mattauer *et al.* 1981, Skjernaa 1989). Thus the presence of sheaths of all scales in the NE Strangways Range is supportive but not diagnostic of non-coaxial shear (Carreras *et al.* 1977, Quinquis *et al.* 1978, Cobbold & Quinquis 1980, Berthé & Brun 1980, Mattauer *et al.* 1981, Lacassin & Mattauer 1985). Furthermore, the symmetrical scatter of both F_2 and F_3 fold axes around L_2 within the S_2 plane is consistent with extreme rotation of fold axes towards L_2 with progressive non-coaxial shear (Sanderson 1973, Escher & Watterson 1974, Bell 1978, Berthé & Brun 1980, Cobbold & Quinquis 1980). The outcrop pattern is analogous to a dome and basin pattern that has been flattened in the S_2 plane and stretched parallel to L_2 so that all limbs and hinges of F_2 and F_3 structures are subparallel. This outcrop pattern cannot be duplicated by refolding any number of isoclinal coaxial fold generations (as discussed earlier), but is analogous to regional-scale deformation by non-coaxial shear.

Low-angle discordance between the major marble unit and adjacent lithological units (Fig. 2) and a consistent east-over-west shear sense throughout the whole area (Fig. 7), imply a regional shear regime involving sub-concordant displacements between lithological units. Such displacements define the S_2 fabric as being a true mylonite (Lister & Snoke 1984) and having formed by non-coaxial shear.

All these features imply that non-coaxial shear operated on all scales in the NE Strangways Range. There is, however, evidence for a component of flattening strain. For example, a component of dilation, between boudins, orthogonal to L_2 within the plane of S_2 and the highly flattened shape of macroscopic sheath folds. However, stretching of M_1 porphyroblasts orthogonal to L_2 is not recognized. Thus the component of flattening

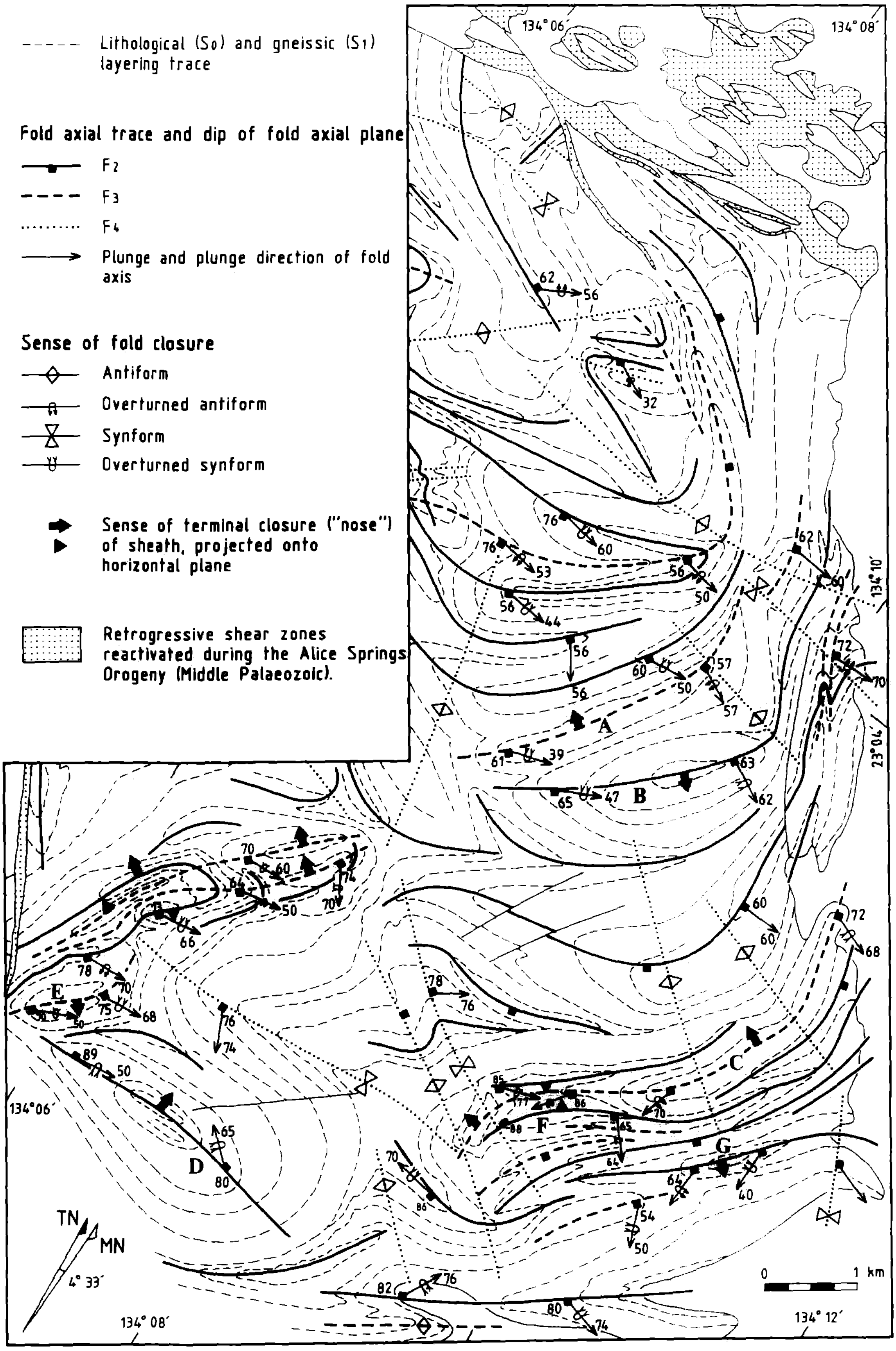

Fig. 11. D_2–D_3 structural interpretation map of the NE Strangways Range.

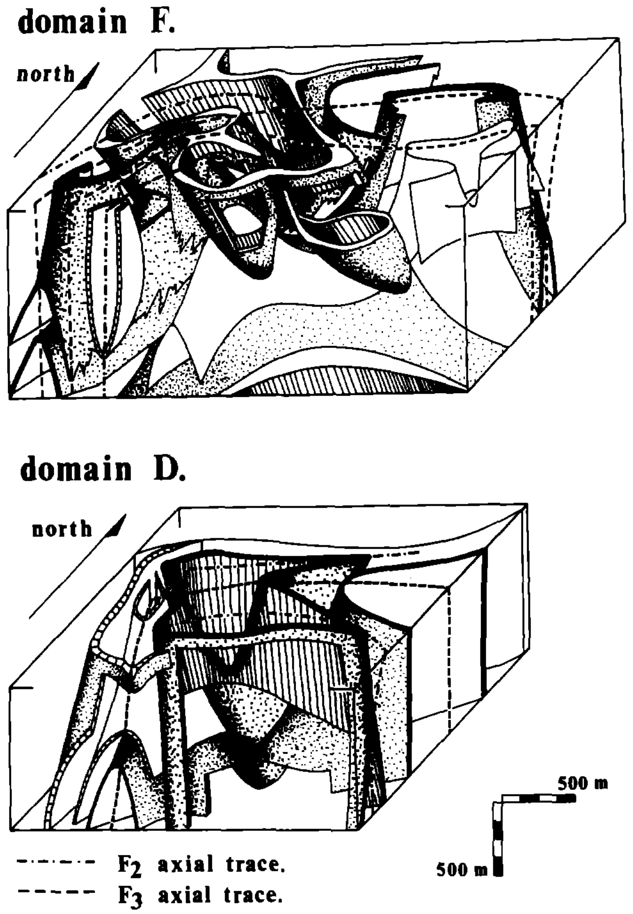

Fig. 12. Three-dimensional block diagrams of lithological form surfaces in two F_2–F_3 fold interference patterns from domains D and F (Fig. 10).

strain was not as significant as the non-coaxial deformation experienced.

Progressive nature of deformation

Co-planarity, co-linearity and the similar style of F_2 and F_3 folds (Figs. 10 and 11), suggest that both D_2 and D_3 are sequential episodes of the same progressive shear deformation. A continuous series of essentially coeval fold generations is postulated where F_2 folds preserve only the first increment of folding. Whereas F_3 folds could potentially comprise many generations of fabricless isoclinal folds (Fig. 6c). Specific generations of F_3 folds could not be correlated throughout the region because of the absence of tectonic fabrics associated with post-F_2 isoclinal folding.

The extensive marble units of the area (Fig. 2) are particularly illustrative of the progressive nature of shear during D_2–D_3. Compositional layering, defined by thin (0.5–10 cm) quartz-rich calc-silicate within the marble, is highly contorted and disrupted (Figs. 6c & d). The discontinuous nature of the layering is due to extreme stretching and boudinage, the tails of which show very ductile thinning (Figs. 6c & d). Calc-silicate layers outline both refolded F_2 and F_3 isoclines and sheath folds, some of which have been refolded through >180° and have formed 'rolling' structures and isolated ball-shaped structures (Figs. 6c & d).

All these features illustrate the highly ductile nature of the carbonate matrix. Consequently, these marble units are interpreted to be zones of considerable high D_2–D_3 shear strain, relative to the surrounding gneisses. The laterally extensive nature of these marble units and low-angle discordances with lithological layering (S_0) in adjacent gneisses (Fig. 2), suggests that these units acted as décollements during D_2–D_3.

Sense of shear

Shear sense during the development of S_2–L_2 fabrics has been derived in thin-section and in the field by *S–C* relationships (Simpson 1984), asymmetrical boudinage (Etchecopar 1974, 1977) and by both σ-type and δ-type porphyroblasts (Passchier & Simpson 1986, Van Der Driessche & Brun 1987). D_2 sense of shear is consistently east-over-west throughout the region (Fig. 7). Shear sense is the same on both limbs of either F_2 and F_3 macroscopic structures (Fig. 7), this feature has also been recorded in the Svecokarelides eastern Finland (Park 1988). The generalized relationships between D_2 shear sense and F_2 and F_3 fold closures (Fig. 9) illustrate the progressive non-coaxial nature of D_2–D_3 deformation.

L_2 lineations define a consistent E–W- to NE–SW-trending axis of transport throughout the Strangways Orogenic Belt as far east as the South Harts Ranges (Fig. 13). Consistent transport direction and sense of shear, in conjunction with identical fold style, fold orientation and nature of tectonic fabrics throughout the Strangways Orogenic Belt (Goscombe 1984, Shaw & Langworthy 1984, Shaw *et al.* 1984b, Norman *et al.* 1989), suggests that the Proterozoic reworking was responsible for deformation of, at least, the Strangways Orogenic Belt portion of the CTP (Fig. 1). Consistent shear sense over such a large region can only be rationalized by some form of crustal scale over-riding of the E–NE over the W–SW.

Bulk shear strain

Qualitatively, the near co-linearity of both F_2 fold axes and marginal hinges of sheath folds with L_2, suggests that the NE Strangways Range has undergone intense shear strain (Sanderson 1973, Coward & Potts 1983). In addition, sheath folds on either mesoscopic or macroscopic scales are uniquely associated with high bulk shear strains ($\gamma > 10$) (Carreras *et al.* 1977, Williams & Zwart 1977, Bell 1978, Lister & Price 1978, Quinquis *et al.* 1978, Minnigh 1979, Berthé & Brun 1980, Cobbold & Quinquis 1980). High bulk shear strains are supported by the very elongate nature (low inter-marginal hinge angles) and flattened ellipse shaped cross-sections (high *B*/*C* ratios) of F_2 and F_3 sheaths (Lacassin & Mattauer 1985). F_3 fold axes are not as tightly constrained around the regional L_2 orientation

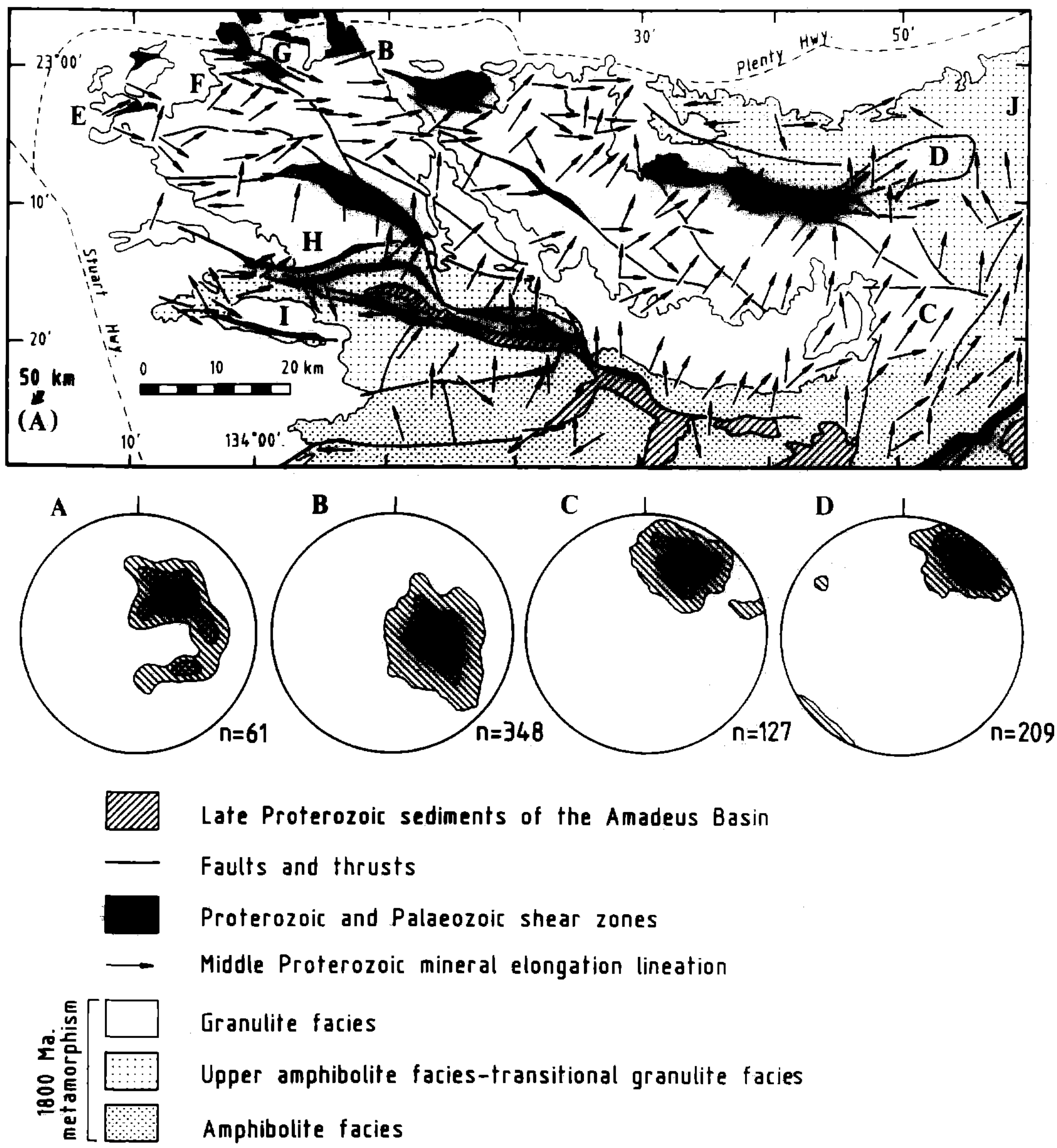

Fig. 13. Plunge direction of Proterozoic mineral elongation lineations (L_2) and peak metamorphic (M_1, 1800 Ma) mineral facies and P–T conditions throughout the Strangways Orogenic Belt. (A) 880–930°C, 6–6.7 kbar, Mt Hay granulites, Glikson (1984). (B) 850–950°C, 8–9 kbar, this study. (C) 760–830°C, 7–8 kbar, Goscombe (1984). (D) 800–860°C, 7–8.5 kbar, Rankin (1983). (E) 840°C, 8 kbar, Windrim (1983). (F) 850–920°C, 8–8.5 kbar, Warren (1983). (G) 850°C, 8 kbar, Warren (1983). (H) 900°C, 8 kbar, Allen & Stubbs (1982). (I) 600°C, 5–6 kbar, Allen & Stubbs (1982). (J) 680–780°C, 6–8 kbar, Oliver *et al.* (1988).

as F_2 folds (Fig. 10), thus the bulk shear strain during D_3 is interpreted to be less than during D_2.

Microstructural fabrics qualitatively illustrate the high bulk shear strains experienced. The acute angle between C and S planes ranges from 7 to 25° suggesting only moderate shear strains. However, most gneisses develop co-planar S–C fabrics. Co-planar S–C foliations are indicative of high shear strains (Berthé *et al.* 1979, Ramsay 1979) and have been suggested to result from shear strains >2.3 (Burg & Laurent 1978). The extreme stretching of garnet, orthopyroxene and feldspar porphyroblasts (Figs. 5a & b), as illustrated by their aspect ratios (Table 2), is illustrative of moderately high shear strains. However, in thin-section the majority of shear strain is considered to have been partitioned by the less viscose matrix of enclosing quartz- and feldspar-aggregate ribbons (Cobbold & Gapais 1983) and by grain boundary recrystallization of M_1 porphyroblasts. The extreme length (≫4 cm) and laterally continuous nature of these aggregate ribbons and the presence of aggregate ribbons of typically more competent phases such as pyroxene, garnet and hornblende, illustrates the high temperature, high shear strain and/or low strain rate, ductile nature of D_2 deformation.

Map-scale sheath fold morphology offers a qualitative illustration of spatial shear strain variation across the NE Strangways Range. The extremely flattened sheath folds in domains C and D (Figs. 2 and 10) are indicative of high shear strain. Furthermore, the degree of grain refinement experienced during D_2 is similarly illustrative of shear strain variation across the area. Domains C and D, in contrast to the rest of the NE Strangways

Table 2. Shape ratios of stretched M_1 porphyroblasts, X is parallel to L_2 and Z is orthogonal to S_2 (Nicolas & Poirier 1976)

		Aspect ratios					
Sample	Augen phase	X/Z	X/Z	Y/Z	$X:Y:Z$	K*	R†
7-415A	orthopyroxene	6.7	2.98	2.25	30:10:4	1.58	4.23
	orthopyroxene	5.3	2.65	2.00	27:10:5	1.65	3.65
	orthopyroxene	4.6	1.84	2.50	18:10:4	0.56	3.34
	orthopyroxene	4.1	2.05	2.00	20:10:5	0.64	3.05
7-415	garnet	4.4	1.76	2.50	18:10:4	0.51	3.26
	garnet	3.5	1.67	2.10	17:10:5	0.61	2.77
6-25	garnet	5.0	3.33	1.50	33:10:7	4.70	3.83
5-87	orthopyroxene	4.7	2.24	2.10	22:10:5	1.13	3.34
	orthopyroxene	3.8	2.11	1.80	21:10:6	1.39	2.91
6-47	K-feldspar	3.0	1.76	1.70	18:10:6	1.10	2.46
	K-feldspar	3.1	1.72	1.80	17:10:6	0.90	2.52
		4.4					
5-425	garnet	3.1	1.55	2.00	16:10:5	0.55	2.55
5-383A	orthopyroxene	3.5					
	orthopyroxene	3.8					
5-314	garnet	2.5	1.70	1.50	17:10:7	1.33	2.20
	K-feldspar	4.2					
5-270D	garnet	3.8	2.50	1.50	25:10:7	3.10	3.00
7-155	garnet	4.0	2.70	1.48	27:10:5	0.30	3.18
		4.4	2.00	2.20	20:10:5	0.80	3.20

*$K = [(X/Y) - 1]/[(X/Y) - 1]$ (Flinn 1962).
†$R = (X/Y) - 1$ (Watterson 1968).

Range, have predominantly mylonitic to ultra-mylonitic S_2–L_2 fabrics in all lithologies, except mafic gneiss. Thus the region east of the major carbonate unit is considered to have partitioned considerably more strain than the rest of the area mapped.

On a smaller scale, there is variation in the shear strain partitioned by different lithologies as illustrated by both the degree of grain refinement and disaggregation of pre-existing S_1 gneissic layering. For example, all marble units are interpreted to have partitioned the greatest shear strains (see earlier discussion). Meta-pelites, quartzo-feldspathic gneiss, orthopyroxene-rich granulite and mafic gneiss partitioned progressively less strain, in that order. Significantly, all lithological boundaries are mylonitized in all domains, suggesting zones of layer-parallel shear between units of differing rheology.

Recumbent vs inclined and extensional vs compressional tectonics

The orientation of the isoclinal folds (D_2–D_3) in the NE Strangways Range at the time of their formation needs to be established. Some ancient high-grade terrains have been shown to have been deformed in a recumbent orientation (Enderby Land, Sandiford 1984; Olary Block, Clarke *et al.* 1986; and the Rayner Complex, Clarke 1987). Whereas most orogens (mountain belts are dominated by inclined to upright structures (e.g. Alps, Himalayas, Appalachians, etc.).

Significant differences in tectonics have been attributed to terrains deformed in recumbent vs inclined environments. Tectonic models for recumbently deformed terrains employ either compressional (very low angle ductile over-riding) (Park 1981, Clarke 1987) or extensional (collapsing crust) (Sandiford 1989) tectonics. Whereas orogens that produced deformational structures of an inclined orientation, can only have involved crustal shortening and so must have formed in a compressional regime. Thus the development of folds in a steeply inclined orientation, uniquely defines deformation as having occurred in a compressional regime.

The well stratified nature of the NE Strangways Range, with laterally continuous and concordant lithological layering (S_0), gneissic layering (S_1), partial melt segregations and orthogneiss units, is interpreted as having comprised a recumbent terrain prior to D_2 (Goscombe 1989). However, the whole of the region is now inclined 50–80° to the ESE. The timing of re-orientation of the NE Strangways Range gneisses is argued to have occurred during D_2–D_3 deformation by compressional tectonics. This is in contrast to D_2–D_3 deformation being recumbent in nature and subsequently tilted into steep orientations by either mega-warping or as fault-bound blocks, during uplift (i.e. during the Alice Springs Orogeny).

Throughout the Strangways Range and as far east as the south Harts Range, both lithological layering and the regional L–S tectonic fabric, consistently dip and plunge to the E or NE (Fig. 13). Thus N–S-trending upright folding on the scale present in the Himalayas (Coward *et al.* 1982) is not recognized. Peak metamorphic conditions, from west to east across the Strangways Orogenic Belt, involve only a 1–2 kbar decrease in pressure and approximately 100–150°C decrease in temperature. Peak metamorphic conditions do not vary significantly across the individual fault-bound blocks

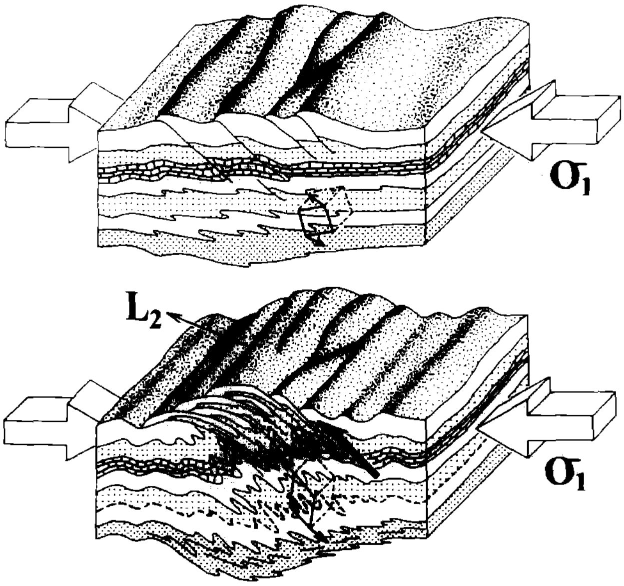

Fig. 14. Schematic cartoon of progressive shear of the crustal lithosphere during the initial stages (D_2–D_3) of the Proterozoic reworking. Dashed line represents the palaeo-M_1 8 kbar isobar after folding by D_2–D_3 deformation, cube represents the NE Strangways Range that is presently exposed at the surface.

that constitute the Strangways Orogenic Belt (Fig. 13). Some of these blocks are up to 50 km wide (in E–W section), thus block rotation of 50–80° to the east, subsequent to the peak of (M_1) metamorphism, would expose a palaeo-M_1 pressure gradient of at least 10 kbar across individual blocks. Such pressure gradients do not exist, thus the Strangways Orogenic Belt as a whole and the fault-bound blocks comprising it, cannot have been tilted significantly.

Consequently, D_2–D_3 structures are responsible for rotating recumbent gneisses into easterly inclined orientations on a local scale (that is, on a macroscopic fold scale). Re-orientation of gneisses by folding on this scale occurred throughout the whole Strangways Orogenic Belt and so gave rise to a steeply inclined terrain while gneisses remained essentially at the same crustal level (Fig. 14). As a corollary of this, D_2–D_3 deformation can only have occurred with concomitant crustal shortening and so must have involved compressional tectonics and crustal thickening. Furthermore, in support of such a model, isostatic rebound in response to crustal overthickening gave rise to a clockwise P–T path during and immediately subsequent to the Proterozoic reworking (Goscombe 1989).

CONCLUSIONS

The NE Strangways Range offers a well-exposed section of middle–lower continental crust that has undergone compressional tectonics at granulite-facies grades. Style and orientation of tectonic elements and the sense of shear during the early episodes (D_2–D_3) of the Proterozoic reworking, are similar over a large portion of the Strangways Orogenic Belt (Rankin 1983, Windrim 1983, Glikson 1984, Goscombe 1984, 1989, Norman *et al.* 1989). Consequently, this analysis of the NE Strangways Range may be typical of the Proterozoic reworking that was experienced by the whole of the Strangways Orogenic Belt.

Bulk shear strains during the initial episodes of the Proterozoic reworking (D_2–D_3) are large and result from predominantly non-coaxial deformation within a regional shear regime involving westerly transport. Non-coaxial deformation is accommodated throughout such a large portion of crust by ductile over-riding and fold repetition. This mechanism of inclined thick skinned tectonics is illustrated by a schematic cartoon in Fig. 14.

Crustal shortening, by such a mechanism, will be manifested in upper-crustal sections by less steeply inclined nappe and thrust sheet stacking. For example, low-angle Proterozoic structuring in the Iwupataka Complex in the south Arunta Block (Amri *et al.* 1987). A decrease in the inclination of deformational structures towards more upper-crustal sections of the Strangways Orogenic Belt supports the model of orogenesis presented above. For example, there is a decrease in plunge of mineral elongation lineations and isoclinal fold axes from the Strangways Range to the south Harts Ranges (Goscombe 1984), with a concomitant decrease in M_1 metamorphic grade (Fig. 13). However, ductile deformation of the middle–lower crust by the mechanism proposed, can only be accommodated, volumetrically, by detachment from the more rheologically rigid upper-mantle lithosphere (Sonder & England 1986, Dunbar & Sawyer 1988).

Acknowledgements—Geoff Clarke, Mike Sandiford, Chris Wilson and Pat James are thanked for helpful discussions. The reviewers are kindly thanked for their helpful comments. This research was undertaken at Melbourne University with the support of an Australian Commonwealth research scholarship and Australian Research Council Grant.

REFERENCES

Allen, A. R. & Black, L. P. 1979. The Harry Creek Deformed Zone, a retrograde schist zone of the Arunta Block, Central Australia. *J. geol. Soc. Aust.* **26**, 17–28.

Allen, A. R. 1979. Metasomatism of a depleted granulite facies terrain in the Arunta Block, Central Australia. 1. Geochemical Evidence. *Contr. Miner. Petrol.* **71**, 85–98.

Allen, A. R. & Stubbs, D. 1982. An $^{40}Ar/^{39}Ar$ study of polymetamorphic complex in the Arunta Block, Central Australia. *Contr. Miner. Petrol.* **79**, 319–332.

Amri, C., Hobbs, B. E. & Ralser, S. 1987. The Iwupataka Complex: A key area of the Proterozoic and Palaeozoic thrust system in the South Arunta Block and its kinematic significance. *Geol. Soc. Aust. Abs.* **19**, 56–57.

Bell, A. M. 1981. Vergence: an evaluation. *J. Struct. Geol.* **3**, 197–202.

Bell, T. H. 1978. Progressive deformation and reorientation of fold axes in a ductile mylonite zone: the Woodroffe thrust. *Tectonophysics* **44**, 285–320.

Berthé, D., Choukroune, P. & Jegouzo, P. 1979. Orthogneiss, mylonite and noncoaxial deformation of granites: the example of the South Armorican Shear Zone. *J. Struct. Geol.* **1**, 31–42.

Berthé, D. & Brun, J. P. 1980. Evolution of folds during progressive shear in the South Armorican Shear Zone, France. *J. Struct. Geol.* **2**, 127–133.

Black, L. P. 1980. Rb–Sr geochronology of the Jervois Range area in the eastern portion of the Arunta Block, N. T. *Bur. Miner. Resour. J. Aust. Geol. Geophys.* **3**, 227–232.

Black, L. P., Shaw, R. D. & Offe, L. A. 1980. The age of the Stuart Dyke Swarm and its bearing on the onset of late Precambrian sedimentation in Central Australia. *J. geol. Soc. Aust.* **27**, 151–155.

Black, L. P., Shaw, R. D. & Stewart, A. J. 1983. Rb–Sr geochronology of Proterozoic events in the Arunta Inlier, central Australia. *Aust. Bur. Miner. Resour. Geol. Geophys. J.* **8**, 129–137.

Burg, J.-P., Iglesias, M., Laurent, Ph., Matte, Ph. & Ribeiro, A. 1981. Variscan intracontinental deformation: the Coimbra–Cordoba shear zone (SW Iberian Peninsula). *Tectonophysics* **78**, 161–177.

Burg, J.-P. & Laurent, Ph. 1978. Strain analysis of a shear zone in a granodiorite. *Tectonophysics* **47**, 15–42.

Carreras, J., Estrada, A. & White, S. 1977. The effect of folding on the *c*-axis fabrics of a quartz mylonite. *Tectonophysics* **39**, 3–24.

Choukroune, P., Gapais, D. & Merle, O. 1987. Shear criteria and structural symmetry. *J. Struct. Geol.* **9**, 525–530.

Choukroune, P. & Lagarde, J. L. 1977. Plans de shistosite et deformation rotationelle: l'exemple du gneiss de champtoceaux (Massif Armoricain) *C.r. hebd. Séanc. Acad. Sci., Paris* **284**, 2331–2334.

Clarke, G. L. 1987. A comparative study of the structural and metamorphic evolution of the Olary (south Australia) and Stillwell Hills (Antarctica) Precambrian terrains. Unpublished Ph.D. thesis, Melbourne University.

Clarke, G. L., Burg, J. P. & Wilson, C. J. L. 1986. Stratigraphic and structural constraints on the Proterozoic tectonic history of the Olary Block, South Australia. *Precambrian Res.* **34**, 107–137.

Cobbold, P. R. & Gapais, D. 1983. Pure shear and simple shear of particle matrix systems with viscosity contrasts (abs.). *Terra Cognita* **3**, 247.

Cobbold, P. R. & Quinquis, H. 1980. Development of sheath folds in shear regimes. *J. Struct. Geol.* **2**, 119–126.

Coward, M. P., Jan, M. Q., Rex, D., Tarney, J., Thirwall, M. & Windley, B. F. 1982. Structural evolution of a crustal section in the western Himalaya. *Nature* **295**, 22–24.

Coward, M. P. & Potts, G. J. 1983. Complex strain patterns developed at the frontal and lateral tips to shear zones and thrust zones. *J. Struct. Geol.* **5**, 383–399.

Dunbar, J. A. & Sawyer, D. S. 1988. Continental rifting at pre-existing lithospheric weaknesses. *Nature* **333**, 450–452.

Escher, A. & Watterson, J. 1974. Stretching fabrics, folds and crustal shortening. *Tectonophysics* **22**, 223–231.

Etchecopar, A. 1974. Simulation par ordinateur de la deformation progressive d'un aggregat polycrystallin. Etude du development de structures orientees par ecrasement et cisaillement. Unpublished Ph.D. thesis, University of Nantes, France.

Etchecopar, A. 1977. A plane kinematic model of progressive deformation in a polycrystalline aggregate. *Tectonophysics* **39**, 121–139.

Flinn, D. 1962. On folding during three-dimensional progressive deformation. *Q. Jl. geol. Soc. Lond.* **118**, 385–433.

Forman, D. J. 1971. The Arltunga Nappe Complex, Macdonnell Ranges, Northern Territory, Australia. *J. geol. Soc. Aust.* **18**, 173–182.

Glikson, A. Y. 1984. Granulite-gneiss terrains of the southwestern Arunta Block, Central Australia: Glen Helen, Narwietooma and Anburla 1:100,000 sheet areas. *Bur. Miner. Resour. Geol. Geophys. Rec.* **22**.

Goscombe, B. D. 1984. The structure, metamorphism, petrology and geochemistry of the Paradise Well area in the Harts Ranges, eastern Arunta Block. Unpublished Honours thesis, Adelaide University.

Goscombe, B. D. 1987. Regional rotational shear accompanying high grade metamorphism in the East Strangways Range, Arunta Block. *Geol. Soc. Aust. Abs.* **19**, 58–59.

Goscombe, B. D. 1989. Structure and metamorphism of the northeast Strangways Range, N.T. Unpublished Ph.D. thesis, Melbourne University.

Hanmer, S. K. 1984. The potential use of planar and elliptical structures as indicators of strain regime and kinematics of tectonic flow. *Geol. Surv. Pap. Can.* **84-1B**, 133–142.

Henderson, J. R. 1981. Structural analysis of sheath folds with horizontal X-axes, northeast Canada. *J. Struct. Geol.* **3**, 203–210.

Hensen, B. J. & Warren, R. G. 1985. Partial melting during granulite metamorphism a mechanism for control of fluid composition? (Abs.) *BMR, Proterozoic Tectonics Conference*, Darwin.

Hobbs, B. E., Means, W. D. & Williams, P. F. 1976. *An Outline of Structural Geology*. John Wiley, New York.

Iyer, S. S., Woodford, F. J. & Wilson, A. F. 1976. Rb–Sr isotopic studies of a polymetamorphic granulite terrane, Strangways Range, central Australia. *Lithos* **9**, 211–224.

James, P. R. & Ding, P. 1987. Field guide to the Harts Ranges area and the Harts Range detatchment zone from the Arunta Inlier of Central Australia. *Geol. Soc. Aust. Arunta Field Workshop*, University of Adelaide.

Lacassin, R. & Mattauer, M. 1985. Kilometre-scale sheath fold at Mattmark and implications for transport direction in the Alps. *Nature* **315**, 739–742.

Lister, G. S. & Price, G. P. 1978. Fabric development in a quartz-feldspar mylonite. *Tectonophysics* **49**, 37–78.

Lister, G. S. & Snoke, A. W. 1984. S–C Mylonites. *J. Struct. Geol.* **6**, 617–638.

Lister, G. S. & Williams, P. F. 1983. The partitioning of deformation in flowing rock masses. *Tectonophysics* **92**, 1–33.

Marjoribanks, R. W. & Black, L. P. 1974. Geology and geochronology of the Arunta Complex north of Ormiston Gorge, Central Australia. *J. geol. Soc. Aust.* **21**, 291–299.

Mattauer, M., Faure, M. & Malavieille, J. 1981. Transverse lineation and large-scale structures related to Alpine obduction in Corsica. *J. Struct. Geol.* **3**, 401–409.

Minnigh, L. D. 1979. Structural analysis of sheath-folds in a meta-chert from the Western Italian Alps. *J. Struct. Geol.* **1**, 275–282.

Mortimer, G. E., Cooper, J. A. & James, P. R. 1985. U/Pb and Rb/Sr geochronology of Proterozoic supracrustals in the vicinity of the Harts Range Ruby Mine, Arunta Inlier, Central Australia (abs.). *BMR Proterozoic Tectonics Conference*, Darwin.

Nicolas, A. & Poirier, J. P. 1976. *Crystalline Plasticity and Solid State Flow in Metamorphic Rocks*. Wiley Interscience, New York.

Norman, A. R., Clarke, G. L. & Vernon, R. H. 1989. The tectonic history of the Strangways Orogenic Belt: a barometric response to late compression. *Geol. Soc. Aust. Abs.* **24**, 106–107.

Oliver, R. L., Lawrence, R., Goscombe, B. D., Ding, P., Sivell, W. J. & Bowyer, D. G. 1988. Metamorphic and crustal considerations in the Harts Range and neighbouring regions, Arunta Inlier. Central Australia. *Precambrian Res.* **40/41**, 277–296.

Park, A. F. 1988. Geometry of sheath folds and related fabrics at the Luikonlahti mine, Svecokarelides, eastern Finland. *J. Struct. Geol.* **10**, 487–498.

Park, R. G. 1981. Origin of horizontal structure in high-grade Archaen terrains. *Spec. Publs geol. Soc. Aust.* **7**, 481–490.

Passchier, C. W. & Simpson, C. 1986. Porphyroclast systems as kinematic indicators. *J. Struct. Geol.* **8**, 831–843.

Platt, J. P. & Vissers, R. M. 1980. Extensional structures in anisotropic rocks. *J. Struct. Geol.* **2**, 397–410.

Quinquis, H., Audren, Cl. Brun, J.-P. & Cobbold, P. R. 1978. Intense progressive shear in Ile de Groix blueschists and compatibility with subduction or obduction. *Nature* **273**, 43–45.

Ramsay, J. G. 1967. *Folding and Fracturing of Rocks*. McGraw-Hill, New York.

Ramsay, J. G. 1979. Shear zones. In: *Proceedings of Conference* 8; *Analysis of Actual Fault Zones in Bedrock. U.S. geol. Surv. Open-file Rep.* **79–1239**, 2–35.

Rankin, L. 1983. Structural geology of the Oonagalabi region N.T. Australia. Unpublished Honours thesis, University of Adelaide.

Sanderson, D. J. 1973. The development of fold axes oblique to the regional trend. *Tectonophysics* **16**, 55–70.

Sandiford, M. 1984. Structural and metamorphic studies in the Fyfe Hills-Khmara bay region, Enderby Land, Antarctica. Unpublished Ph.D. thesis, University of Melbourne.

Sandiford, M. 1989. Horizontal structures in granulite terrains: a record of mountain building or mountain collapse. *Geology* **17**, 449–452.

Shaw, R. D. & Langworthy, A. P. 1984. Strangways Range region, Northern Territory. *Aust. Bur. Miner. Resour. Geol. Geophys.*, 1:100,000 Geological Map Commentary.

Shaw, R. D., Stewart, A. J. & Black, L. P. 1984a. The Arunta Inlier: a complex ensialic mobile belt in central Australia. Part 2: tectonic history. *Aust. J. Earth Sci.* **31**, 457–484.

Shaw, R. D., Stewart, A. J. & Rickard, M. J. 1984b. Arltunga–Harts Range region, Northern Territory. *Aust. Bur. Miner. Resour. Geol. Geophys.*, 1:100,000 Geological Map Commentary.

Shaw, R. D. & Wells, A. T. 1983. Alice Springs (second edition), Northern Territory 1:250,000 Geological series. *Aust. Bur. Miner. Resour. Geol. Geophys., Explan. Notes* **SF/53–14**.

Simpson, C. & Schmid, S. M. 1983. An evaluation of criteria to deduce the sense of movement in sheared rocks. *Bull. geol. Soc. Am.* **94**, 1281–1288.

Simpson, C. 1984. Borrego Springs–Santa Rosa mylonite zone: a Late Cretaceous west-directed thrust in southern California. *Geology* **12**, 8–11.

Skjernaa, L. 1989. Tubular folds and sheath folds: definitions and conceptual models for their development, with examples from the Grapesvare area, northern Sweden. *J. Struct. Geol.* **11**, 689–703.

Sonder, L. J. & England, P. 1986. Vertical averages of rheology of the continental lithosphere: relation to thin sheet parameters. *Earth Planet. Sci. Lett.* **77**, 81–90.

Stewart, A. J., Shaw, R. D. & Black, L. P. 1984. The Arunta Inlier: A complex ensialic mobile belt in central Australia. Part 1: stratigraphy, correlations and origin. *Aust. J. Earth Sci.* **31**, 445–455.

Teyssier, C. 1985. A crustal thrust system in an intracratonic tectonic environment. *J. Struct. Geol.* **7**, 689–700.

Thiessen, R. 1986. Two-dimensional refold interference patterns. *J. Struct. Geol.* **8**, 563–573.

Van Der Driessche, J. & Brun, J.-P. 1987. Rolling structures at large shear strain. *J. Struct. Geol.* **9**, 691–704.

Warren, R. G. 1983. Metamorphic and tectonic evolution of granulites Arunta Block, Central Australia. *Nature* **305**, 300–303.

Watterson, J. 1968. Homogeneous deformation of the gneisses of Vesterland S.W. Greenland. *Medd. Grønl.* **175** (6).

Wells, A. T. & Moss, F. J. 1983. The Ngalia Basin, Northern Territory: Stratigraphy and structure. *Bull. Bur. Miner. Resour.* **212**.

Williams, P. F. & Zwart, H. J. 1977. A model for the development of the Seve-Koli Caledonian nappe complex. In: *Energetics of Geological Processes* (edited by Saxena, S. K. & Bhattacharji, S.). Springer, New York, 169–187.

Windrim, D. P. 1983. Chemical and thermal evolution of Strangways granulites Central Australia. Unpublished Ph.D. thesis, Australian National University, Canberra.

Windrim, D. P. & McCulloch, M. T. 1986. Nd and Sr isotopic systematics of central Australian granulites: chronology of crustal development and constraints on the evolution of lower continental crust. *Contr. Miner. Petrol.* **94**, 289–303.

Woodford, P. J., Mateen, A., Green, D. C. & Wilson, A. F. 1975. $^{40}Ar/^{39}Ar$ geochronology of a high-grade polymetamorphic terrain, northeastern Strangways Range, central Australia. *Precambrian Res.* **2**, 375–396.